



Research paper

Controllable fabrication of a novel porous Ni-alginate hybrid material for hydrogenation



Xianliang Qiao, Libo Niu, Huiling Zhang, Xin Wen, Yingying Cao, Guoyi Bai*

Key Laboratory of Chemical Biology of Hebei Province, College of Chemistry and Environmental Science, Hebei University, Baoding 071002, PR China

ARTICLE INFO

Article history:

Received 5 April 2017

Received in revised form 2 June 2017

Accepted 29 June 2017

Available online 30 June 2017

Keywords:

Hybrid material

Sodium alginate

Nickel

Hydrogenation

Stability

ABSTRACT

A novel porous Ni-alginate hybrid material was fabricated via a facile in-situ reduction of a Ni(II) alginate 3D hydrogel, which was obtained through the coordination of Ni(II) ions with sodium alginate, a natural polysaccharide. Notably, Ni(II) species first coordinated with Alg as the gelling agent during the construction of the 3D hydrogel and then were reduced to the active Ni(0) species in hybrid materials for hydrogenation. TEM results revealed that the Ni particles in Ni-alginate hybrid material were highly dispersed and in extremely small sizes, compared with those in the alginate supported Ni catalyst prepared by a conventional impregnation-reduction method. XPS and TGA results demonstrated the strong interaction between Ni and alginate in Ni-Alg-0 (where "Alg" represents sodium alginate and "0" represents the volume of water added in the NaBH₄ solution during reduction), which suppresses agglomeration and prevents loss of the active species. This novel catalyst exhibited excellent catalytic activity and stability in styrene hydrogenation with no appreciable loss of its initial activity for up to 20 times of recycling. Furthermore, this material exhibited good catalytic activity in the hydrogenation of a number of unsaturated substrates as well.

© 2017 Elsevier B.V. All rights reserved.

1. Introduction

In recent decades, nanomaterials have attracted much attention due to their unique surface properties and size-dependent quantum effects. Functional nanomaterials are widely used in many fields such as biomedicine and catalysis [1–6]. Highly active and stable nanocatalysts are the key requirements for the actual applications of nanomaterials in a catalytic system. Much effort has been devoted to improve the activity and stability of nanocatalysts by adding dispersing agents or stabilizers, such as carboxylates [7,8], surfactant [9] and polymers [10–12], during the catalyst preparation. For example, Herbois et al. have improved the activity and stability of Ru particles in furfural hydrogenation by using cyclodextrins and polyvinylpyrrolidone (PVP) as the co-dispersants [13]. To further improve the stability of nanocatalysts, the active species were loaded onto a variety of porous materials, such as porous silicon [14,15], ZrO₂ [16], Al₂O₃ [17,18] and porous carbon [19], to prepare the supported nanocatalysts. For example, Xia et al. have prepared N-doped porous carbon supported Pd as a highly dispersed and efficient catalyst for aromatic hydrogenation [20]. However, the methods described above still have some disadvan-

tages, such as high cost, time-consuming or pollutive preparation processes. Meanwhile, removal of the stabilizing molecules is problematic and may lead to changes in the size and shape of the nanoparticles [21,22]. In addition, the uniform dispersion of the active species on supports is somewhat difficult to achieve [23,24]. Therefore, it is highly desirable to develop a simple, green and low-cost approach to prepare nanocatalysts with high activity and good stability.

Natural polysaccharide hydrogels, especially alginate hydrogels, have attracted considerable attention because of their environmental sustainability, unique opened porous structure, high surface areas, various functionalities and extensive solvent stability. Functionalized hydrogel has been demonstrated to be an exciting green support for the immobilization of metal particles [25–28]. In particular, one fascinating property of alginate is its selective ionic coordinations with multivalent ions and subsequent transformation into a macromolecular hydrogel with a special 3D network structure [29–31]. For example, Primo et al. have presented an interesting work on the synthesis of Pd particles grown on 3D Ca(II) alginate hydrogels that exhibited good catalytic performance in the Suzuki reaction [30]. However, all the active species need to be loaded on the previously constructed hydrogels to take advantage of the 3D network, and most of the current researches were limited to aqueous phase or noble metal. To the best of our knowledge, there was no report on the fabrication of a 3D alginate

* Corresponding author.

E-mail address: baiguoyi@hotmail.com (G. Bai).



Fig. 1. Schematic illustration for the fabrication of Ni-Alg-x.

hydrogel-based nanocomposite, which can be used as an efficient hydrogenation catalyst after in-situ reduction.

Recently, Li et al. have reported a facile one-pot route for the synthesis of Pd@MOF composites without additional stabilizing agents, which showed high activity and chemoselectivity in the hydrogenation of cinnamaldehyde [32]. Inspired by their work, we first fabricated a crosslinked 3D hydrogel through the coordination of $\text{Ni}(\text{II})$ ions with sodium alginate (Alg), and then a novel porous Ni-alginate (Ni-Alg) hybrid material with highly dispersed Ni particles was obtained via a facile in-situ reduction. $\text{Ni}(\text{II})$ species first coordinated with Alg as the gelling agent during the construction of the 3D hydrogel and then were reduced to $\text{Ni}(0)$ species in hybrid materials for further hydrogenation. Interestingly, the morphology and the Ni particle sizes of the hybrid materials can be tuned by altering the solvent components during the reduction process. The well organized hybrid material showed excellent catalytic activity in styrene hydrogenation due to its high Ni dispersion and small particle size. Particularly, the strong interaction between Ni particles and Alg can suppress agglomeration and prevent loss of the active Ni species in the hydrogenation process, resulting in an enhanced stability of this material. The relationship between the structure and catalytic property of this novel hybrid material was clarified based on necessary characterizations.

2. Experimental section

2.1. Chemicals and reagents

Unless otherwise stated, all reagents were purchased from Baoding Huixin Reagent and Apparatus Co., Ltd. and were used as received without further purification. Ultrapure Ar (99.999%) and 5 vol% H_2/N_2 were purchased by Baoding Zhuoda Gas Co. Ltd.

2.2. Preparation of catalytic materials

The $\text{Ni}(\text{II})$ alginate 3D hydrogel was prepared by an ionic induced crosslinking method, as shown in Fig. 1. Typically, 2.0 g of sodium alginate powder was first dissolved in 98 mL deionized water and stirred for 12 h at room temperature to afford a transparent and viscous solution. It was kept for 2 h to remove the residual bubbles, and then dropped to a $\text{NiCl}_2 \cdot 6\text{H}_2\text{O}$ solution (0.2 M, 50 mL) under constant stirring. Light-green $\text{Ni}(\text{II})$ alginate gel beads were immediately formed (Fig. 1a) and further kept in the same solution for another 12 h. Subsequently, the gel beads were separated and washed with distilled water to remove excess $\text{Ni}(\text{II})$ ions. Then, the solvent was exchanged from water to ethanol and the gel beads were stored in ethanol for further use. After that, 2.0 g gel beads were immersed into 40 mL 0.066 M NaBH_4 solution (ethanol solution or a mixture of ethanol and water) to reduce the $\text{Ni}(\text{II})$ ions, followed by agitation at 0 °C for 5 h. Finally, the resulted black composites were washed and then activated in ethanol with 1 MPa H_2 at 100 °C for 1 h. The obtained hybrid materials were denoted as Ni-Alg-x, where Alg represents sodium alginate and x (x = 0, 5, 10, respectively) represents the volume (mL) of water added in the NaBH_4 solution. The Ni loadings of Ni-Alg-x were about 5.8 wt% based on the inductively coupled plasma (ICP) results. Furthermore, hybrid materials with different concentration of $\text{NiCl}_2 \cdot 6\text{H}_2\text{O}$ solution (0.1 M, 0.4 M, and 0.8 M) were prepared by the same method as Ni-Alg-0 and their Ni loadings were identified to be 3.6 wt% (0.1 M), 11.5 wt% (0.4 M) and 15.8 wt% (0.8 M), respectively. In addition, the conventional alginate supported Ni catalyst was prepared by an impregnation-reduction method. Typically, $\text{NiCl}_2 \cdot 6\text{H}_2\text{O}$ was dissolved in ethanol, and then sodium alginate powder was added into this solution. The mixture was first treated under ultrasound for 0.5 h and then dried at 120 °C for 5 h. Subsequently, 40 mL 0.066 M NaBH_4 ethanol solution was dropped to reduce the $\text{Ni}(\text{II})$ ions, followed by agitation at 0 °C for 5 h. The supported catalyst was finally obtained after washing and activation as described above

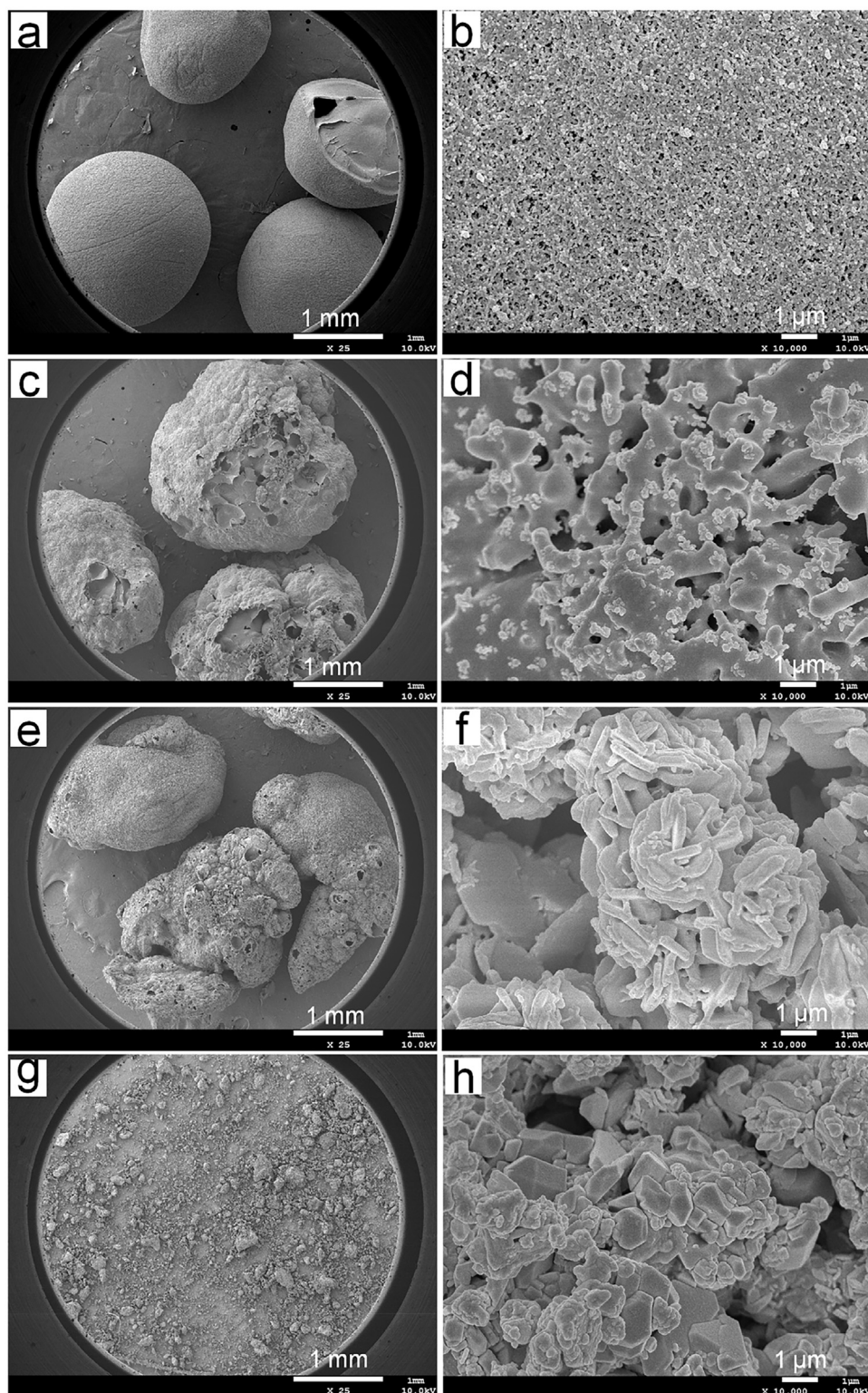


Fig. 2. SEM images of Ni-Alg-0 (a and b), Ni-Alg-5 (c and d), Ni-Alg-10 (e and f) and Ni/Alg-0 (g and h).

and denoted as Ni/Alg-0. Moreover, Ni particles were prepared by a similar method described in our previous work [33].

2.3. Catalyst characterization

Scanning electron micrographs (SEM) were obtained on a JEOL JSM-7500 instrument. X-ray diffraction (XRD) patterns were

recorded on a Bruker D8-Advance X-ray diffractometer using a Cu K α radiation source. Transmission electron microscopy (TEM), high-resolution transmission electron microscopy (HRTEM) and selective-area electron diffraction (SAED) were carried out on a FEI Tecnai G2 F20 microscope. Brunauer-Emmett-Teller (BET) surface area and pore volume were obtained on a Micromeritics Tristar II 3020 surface area and pore analyzer. Fourier transform

infrared spectra (FT-IR) were recorded on a Bruker VERTEX 70 Fourier transform spectrometer using KBr pellets. ICP was carried out using a Varian Vista-MPX spectrometer. H₂-chemisorption and temperature-programmed desorption of hydrogen (H₂-TPD) were carried out on a TP-5000 instrument equipped with a thermal conductivity detector. Thermogravimetric analysis (TGA) was performed on a Perkin-Elmer Pyris 6 type thermogravimetric analyzer under nitrogen atmosphere (20 mL min⁻¹) at a heating rate of 10 °C min⁻¹. X-ray photoelectron spectroscopy (XPS) analysis was carried out on a PHI 1600 spectrometer using Mg K α X-ray source for excitation and the data processing software was MultiPak V6.1A.

2.4. Catalyst activity tests

Hydrogenation of styrene was performed as follows: ethanol (40 mL), catalyst (0.36 g) and styrene (5.0 mL, 42 mmol) were successively added into a 100 mL Parr 4598 HPHT stainless steel autoclave equipped with a mechanical stirrer and an electrical heating system. The autoclave was first flushed with H₂ five times, followed by evacuation, to displace residual air, and then pressurized with H₂ to 2.0 MPa and heated to the requisite temperature. On reaching the required temperature, the reaction was started by stirring the reaction mixture vigorously and allowed to proceed for 0.5 h. When the reaction was complete, the reaction mixture was allowed to cool to room temperature and the catalyst was separated by filtration for recycling. Hydrogenations of other unsaturated substrates were performed under the same reaction conditions unless otherwise stated. The reaction solutions were analyzed by Agilent 7820A gas chromatography (GC) and the structures of the products were identified using gas chromatography-mass spectroscopy (GC-MS) on an Agilent 5977A spectrometer.

3. Results and discussion

3.1. Preparation of Ni-Alg-x hybrid materials

The nickel alginate 3D hydrogel was first prepared through the coordination of Ni(II) ions with the abundant carboxyl groups along the Alg chains [34]. The Ni(II) ions could be further captured and fixed by the carboxyl groups in the 3D hydrogel network, resulting in their high dispersion (Fig. 1a). Then, Ni-Alg-x porous hybrid materials with highly dispersed Ni particles can be fabricated by a facile in-situ reduction (Fig. 1b). In these Ni-Alg-x hybrid materials, Alg can serve as “skeleton” to support the porous structure and suppress the agglomeration of the highly dispersed Ni particles.

During the reduction process, solvent was found to play an important role in the fabrication of the hybrid materials. When the reduction was carried out in water, the hydrogel became gradually softer and softer, and then slowly dissolved to produce viscous mixture during the reduction process (Fig. S1b). In contrast, when ethanol was used as the solvent, the hydrogel could be retained due to the insolubility of Alg in ethanol (Fig. S1c), accounting for the efficient fabrication of the required hybrid materials. Considering the important impact of solvent, the formation mechanism of Ni-Alg-x was then investigated by altering the water content in the NaBH₄ ethanol solution during the reduction process. It was obvious that the morphologies of the hybrid materials with different water content were markedly different (Fig. 2). As can be seen, Ni-Alg-0 was spherical with a diameter of about 1.5 mm (average size of 30 beads, Fig. 2a) and consisted of interconnected fibrils (Fig. 2b). However, the hybrid materials gradually lost their shapes with the increase of water content. Ni-Alg-5 and Ni-Alg-10 both exhibited irregular shapes (Fig. 2c and e) with rod- and flake-like structures, respectively (Fig. 2d and f). In contrast, the supported Ni/Alg-0 showed markedly different morphology (Fig. 2g and h),

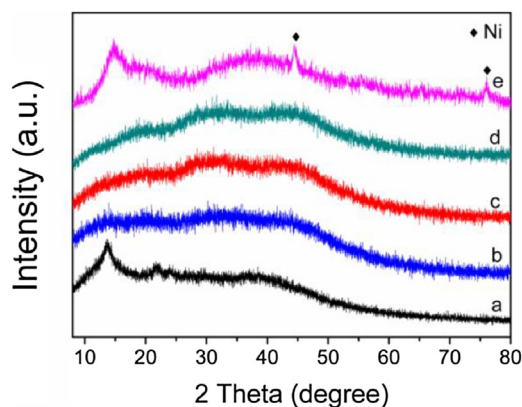


Fig. 3. XRD patterns of Alg (a), Ni-Alg-0 (b), Ni-Alg-5 (c), Ni-Alg-10 (d) and Ni/Alg-0 (e).

compared to the hybrid materials. Moreover, the Ni loadings also have a great impact on the morphologies and structural properties of the hybrid materials (Fig. S2, Table S1). With the increase of the Ni(II) concentrations, the BET surface areas increased, the pore sizes decreased, and the networks became denser and denser.

Considering the good solubility of Alg in water, we assumed that it should be first hydrated and then slowly dissolved during the reduction of Ni(II) ions, when water was added into the reducing solution [35]. This was attributed to the decrease in the number of reticulation sites, resulting in the destruction of the network structure (Fig. 1c) [30], as demonstrated by the emergence of the rod- and flake-like structures in Ni-Alg-5 and Ni-Alg-10. In contrast, when pure ethanol was used as the solvent, the Alg structural unit could be in-situ “frozen” rather than dissolved, thus generated a desired hybrid material with the reduced Ni particles, accounting for the preservation of its porous structure, in agreement with the SEM results. Therefore, the insolubility of Alg in ethanol was essential to construct and maintain this porous hybrid material, which was beneficial for the high dispersion of Ni particles.

3.2. Characterization of materials

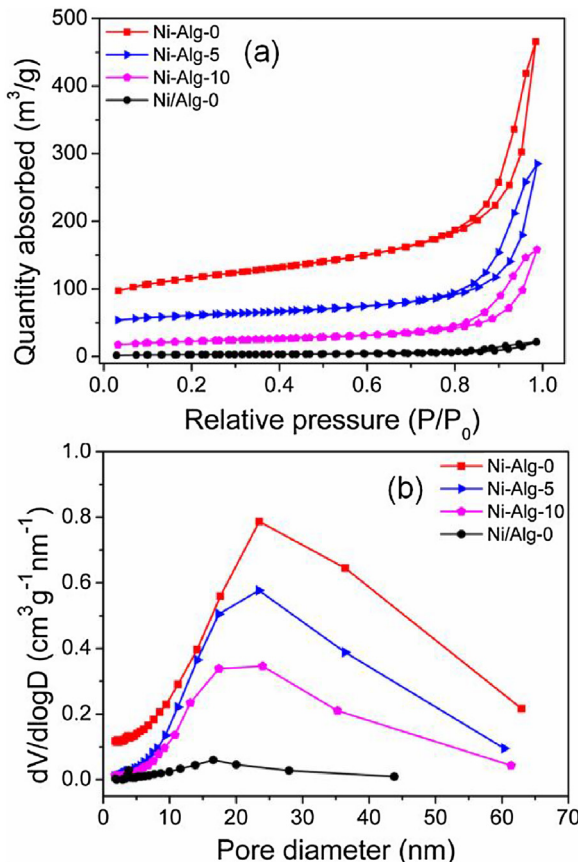
Wide-angle XRD patterns of Alg, Ni-Alg-x and Ni/Alg-0 are shown in Fig. 3. As can be seen, Alg exhibited three characteristic peaks at 14.5°, 21.6°, and 36.7° (curve a) [36,37]. However, these peaks, especially the peak at 14.5°, disappeared in all Ni-Alg-x hybrid materials, demonstrating the destruction of Alg structure. This was attributed to the reduction of the nickel species, leading to the creation of more disorder in the system [38,39]. In contrast, characteristic diffraction peaks of Alg were still clearly observed in Ni/Alg-0 (curve e), indicating the retention of its structure in this conventional supported catalyst. Particularly, two new diffraction peaks appeared in Ni/Alg-0 at 44.5° and 76.1°, suggesting the existence of the crystalline Ni [40]. However, except a single broad peak at around 2θ = 45°, no obvious characteristic diffraction peaks related to crystalline Ni can be observed in Ni-Alg-x, which could be attributed to the amorphous state or high dispersion of Ni in these hybrid materials [41]. Similar results have also been reported in other metal-alginate materials [42]. A successive diffraction halo in the SAED image of Ni-Alg-0 further demonstrated its amorphous state (Fig. S3B) [43]. Furthermore, only one sole diffraction peak at about 2° was observed in the low-angle XRD pattern of Ni-Alg-0 (Fig. S3C), indicating its mesoporous nature.

Ni loadings, Brunauer-Emmett-Teller (BET) surface areas, pore volumes, H₂-chemisorptions, conversion and turnover frequency (TOF) of Ni-Alg-x and Ni/Alg-0 were measured, and the results are summarized in Table 1. As can be seen, the Ni loadings of all mate-

Table 1

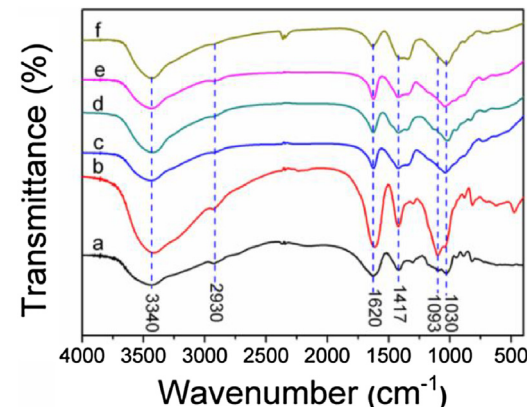
Structural properties and catalytic performances of different materials.

Sample	Ni loading ^a (wt%)	Surface area ($\text{m}^2 \text{ g}^{-1}$)	Pore volume ($\text{cm}^3 \text{ g}^{-1}$)	H_2 -chemisorption ($\text{cm}^3 \text{ g}^{-1}$)	Conversion ^b (%)	TOF ^c (10^3 h^{-1})
Ni-Alg-0	5.8	174	0.61	0.114	93.2	10.4
Ni-Alg-5	5.8	75	0.38	0.105	85.7	8.1
Ni-Alg-10	5.9	46	0.23	0.082	80.5	7.0
Ni/Alg-0	6.1	9	0.03	0.078	81.1	7.2

^a Based on ICP results.^b Reaction conditions: styrene (42 mmol), ethanol (40 mL), catalyst (0.36 g), $\text{P}(\text{H}_2)=2 \text{ MPa}$, 300 rpm, 100 °C, 20 min.^c The TOF values were calculated based on the conversion of styrene in 10 min, according to the reference [44].**Fig. 4.** N_2 adsorption–desorption isotherms (a) and pore size distributions of the different materials (b).

rials are similar based on the ICP results. As for Ni-Alg-x, the surface areas, pore volumes and H_2 -chemisorption values decreased gradually with the increase of the water content during the reduction, demonstrating that the addition of water has destroyed the porous structure of these hybrid materials. Furthermore, Ni-Alg-0 exhibited markedly higher surface area, pore volume, H_2 -chemisorption and TOF value than the conventional supported catalyst Ni/Alg-0, which can be attributed to its porous nature and highly dispersed active species.

N_2 adsorption–desorption isotherms and pore size distributions of the prepared materials are shown in Fig. 4. All isotherms of Ni-Alg-x exhibited typical IV type isotherms with a H3 hysteresis loop at relatively higher pressure, probably due to the capillary condensation phenomenon, demonstrating the successful formation of mesopores (Fig. 4a) [45]. Meanwhile, their pore size distributions presented broad peak centered around 23 nm, also confirming their mesoporous structure (Fig. 4b), in agreement with the low-angle XRD result of Ni-Alg-0 (Fig. S3C). In contrast, the isotherm and pore size distribution of Ni/Alg-0 are markedly different from those Ni-Alg-x hybrid materials, indicating its poor pore nature.

**Fig. 5.** FT-IR spectra of Alg (a), Ni(II) alginate gel (b), Ni-Alg-0 (c), Ni-Alg-5 (d), Ni-Alg-10 (e) and Ni/Alg-0 (f).

FT-IR spectra of Alg, Ni(II) alginate gel, Ni-Alg-0, Ni-Alg-5, Ni-Alg-10 and Ni/Alg-0 are presented in Fig. 5. Most of the characteristic peaks of Alg were observed in all prepared materials. In the spectrum of Alg, the broad peaks at about 3340 cm^{-1} were assigned to the stretching vibrations of O–H, and the weak absorption bands at about 2930 cm^{-1} were attributed to the stretching vibrations of C–H. The peaks at about 1620 and 1417 cm^{-1} were associated with the asymmetric and symmetric stretching vibrations of the carboxyl groups, respectively; while the two absorption bands at about 1093 cm^{-1} and 1030 cm^{-1} belonged to the C–O–C groups of the saccharide structure [46,47]. Notably, the characteristic peak at 1620 cm^{-1} was shifted to a lower wavenumber of 1605 cm^{-1} in the spectrum of Ni(II) alginate gel, indicating the coordination of Ni(II) with carboxyl groups [48], which could benefit not only the high dispersion but also the reduction rate control of Ni(II) ions.

XPS spectra of Ni 2p in Ni-Alg-0 and Ni/Alg-0 are shown in Fig. 6. Generally, the binding energies of Ni 2p_{3/2} in metallic Ni and Ni(II) are around 852 and 855 eV, respectively [49,50]. Thus, the peaks at 852.34 and 852.67 eV can be ascribed to the metallic Ni, and the peaks at 855.68 and 855.83 eV mainly ascribed to Ni(OH)₂ [51]. Considering that the binding energies of Ni 2p in Ni-Alg-0 were lower than those in Ni/Alg-0 and the binding energy of O 1s in Ni-Alg-0 was 0.42 eV higher than that in Ni/Alg-0 (Fig. S4d), there should be certain charge transfer from Alg to the Ni atom, probably via the C=O group [52]. These results indicated that there should be stronger interaction between Ni and Alg in Ni-Alg-0 than that in Ni/Alg-0 [49]. Furthermore, there was more metallic Ni (45.6%) in Ni-Alg-0 than that (28.7%) in Ni/Alg-0. In addition, more surface metallic Ni can be obtained with the increase of Ni loadings (Table S2), which can be attributed to the reduction of more excessive free Ni(II) ions in hydrogels.

On the other hand, the peaks at 188.14 and 187.96 eV in B 1s spectra can be ascribed to the elemental B, and the peaks at 191.25 and 191.75 eV ascribed to the oxidized B (Fig. S4a and b). The B 1s of the elemental B in either Ni-Alg-0 or Ni/Alg-0 exceeds that of pure B

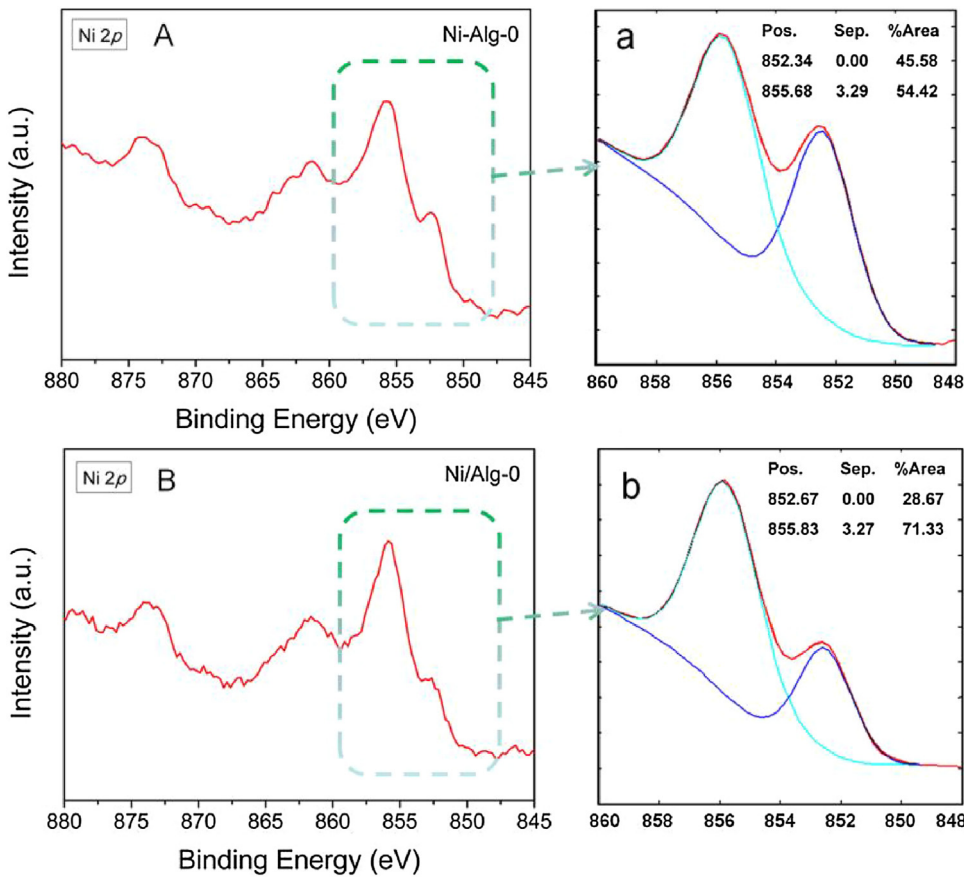


Fig. 6. XPS spectra of Ni 2p in Ni-Alg-0 (A, a) and Ni/Alg-0 (B, b).

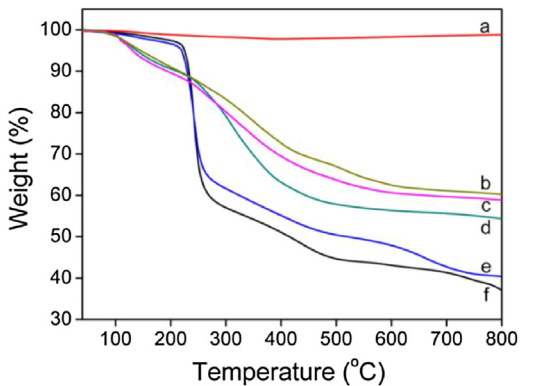


Fig. 7. TGA curves of Ni (a), Ni-Alg-0 (b), Ni-Alg-5 (c), Ni-Alg-10 (d), Ni/Alg-0 (e) and Alg (f).

(187.1 eV) by 0.8–1.0 eV [53], indicating the electrons transfer from B to Ni, which is beneficial for improving the activity of the catalyst.

Fig. 7 shows the TGA curves of Ni, Ni-Alg-0, Ni-Alg-5, Ni-Alg-10, Ni/Alg-0 and Alg in N₂ gas flow. As can be seen, Ni particles (curve a) was stable, Alg (curve f) exhibited four steps of weight loss in the range of 0–800 °C, including desorption of adsorbed water (<220 °C), dehydration and decarboxylation (220–280 °C) and degradation of some polymers (300–500 °C and 700–800 °C) [54]. Additionally, it maintained a weight percent of over 35% in this temperature range, similar to the previous report [38]. Apparently, the weight losses of Ni-Alg-x (curve b–d) were much lower than Alg, indicating their greater heat stability compared with Alg [55]. In contrast, the weight loss trend of Ni/Alg-0 (curve e) was very similar to that of Alg, indicating its poor heat stability. More impor-

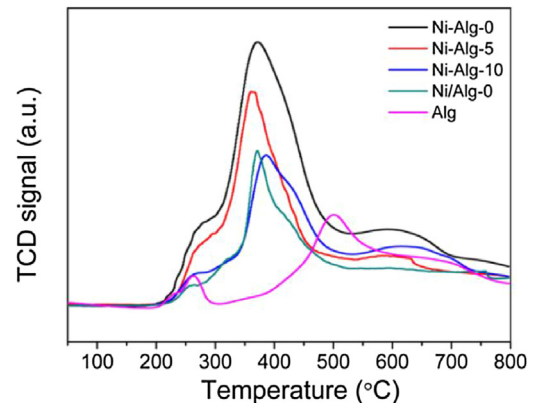


Fig. 8. H₂-TPD profiles of Alg, Ni-Alg-0, Ni-Alg-5, Ni-Alg-10 and Ni/Alg-0.

tantly, the residual weight of Ni-Alg-x (about 58%) was higher than Ni/Alg-0 (about 40%), demonstrating that there existed stronger interaction between Ni and Alg in Ni-Alg-x than Ni/Alg-0, which could result in better stability in hydrogenation [56]. In addition, the thermal stability of Ni-Alg-0, Ni-Alg-5 and Ni-Alg-10 gradually decreased, which should be attributed to the gradual destruction of the porosity and homogeneity of these hybrid materials with the increase of water content during the reduction, as proven by previous SEM results.

H₂-TPD profiles of Alg, Ni-Alg-0, Ni-Alg-5, Ni-Alg-10 and Ni/Alg-0 are shown in **Fig. 8**. The purpose for the presentation H₂-TPD profile of the Alg is to eliminate the interference of Alg thermal decomposition in Ni-Alg-x and Ni/Alg-0. The peaks at approximately 250, 500 and 650 °C should be ascribed to the thermal

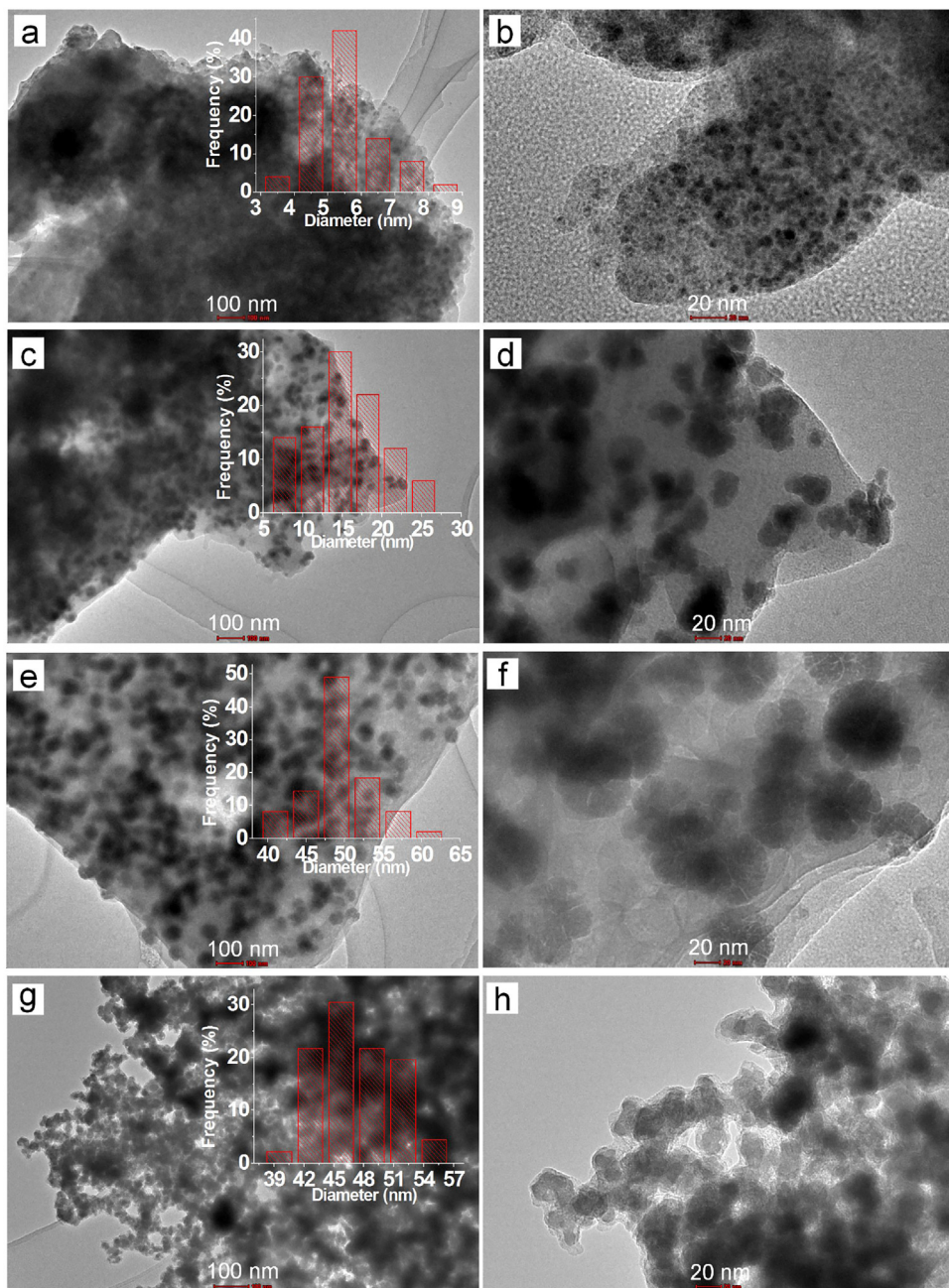


Fig. 9. TEM images and particle size distributions of Ni-Al-0 (a and b), Ni-Alg-5 (c and d), Ni-Alg-10 (e and f) and Ni/Alg-0 (g and h).

decomposition of Alg, as demonstrated by the TGA results [54]. Obviously, Ni-Alg-0 exhibited the largest hydrogen desorption peak at a relatively lower temperature, indicating a higher Ni dispersion and more surface dissociated hydrogen in this sample [57]. Both Ni-Alg-5 and Ni-Alg-10 showed smaller hydrogen desorption peaks, which could be attributed to the hydrogen adsorbed on bulk or relatively poorly-dispersed Ni particles. These results are in good agreement with the H₂-chemisorption results in Table 1. In contrast, Ni/Alg-0 exhibited the smallest hydrogen desorption peak, indicating its relatively low capacity of hydrogen adsorption. Thus, the high adsorption capacity and low desorption temperature of chemisorbed hydrogen is believed to be beneficial for the good catalytic activity of Ni-Alg-0 [58].

TEM images and particle size distributions of Ni-Alg-0, Ni-Alg-5, Ni-Alg-10 and Ni/Alg-0 are shown in Fig. 9. It was obvious that all Ni particles were well dispersed in Ni-Alg-x hybrid materials (a-f),

which can be ascribed to the coordination of Ni(II) ions with Alg in gelation stage. Notably, Ni-Alg-0 showed a relatively narrow Ni particles distribution of 3–9 nm with an average size of 5.5 nm (a and b). However, the particle growths were apparent in Ni-Alg-5 and Ni-Alg-10 (c–f), resulting in a relatively wider particles distribution of 7–26 nm and 40–62 nm with a bigger average size of 16 nm and 46 nm, respectively. We attributed this phenomenon to the assembling of some primary Ni particles to form larger ones, caused by the destruction of the network structure in the reduction process (Fig. 1c). Interestingly, the Ni particles in Ni-Alg-10 showed a special petal-like structure (f), demonstrating the assembly of the Ni particles [59]. In contrast, the Ni dispersion is rather poor in Ni/Alg-0 (g and h) and its average size (47.3 nm) is much bigger than that of Ni-Alg-0 (5.5 nm).

Additionally, as can be seen from the HRTEM and SAED results (Fig. S3B), Ni(0) species presented in an amorphous state in Ni-Alg-

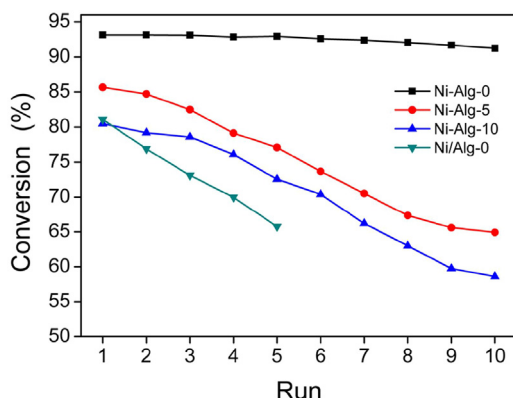


Fig. 10. Reusability results of Ni-Alg-x and Ni/Alg-0. Reaction conditions: styrene (42 mmol), catalyst (0.36 g), ethanol (40 mL), $P(H_2)=2$ MPa, 300 rpm, 100 °C, 20 min.

0, and in contrast, crystalline Ni(0) formed in Ni/Alg-0. We ascribed these results to the fact that the reduction rate of Ni(II) in Ni-Alg-0 was slower than that in Ni/Alg-0 due to the coordination of Ni(II) ions with alginate, resulted in an amorphous state of Ni particles, while the reduction of Ni(II) was carried out at a relatively low temperature (0 °C).

3.3. Catalytic performances of materials

Catalytic performances of these materials were tested in the hydrogenation of styrene, and the results are listed in Table 1. As can be seen, Ni-Alg-0 exhibited an excellent catalytic performance with the conversion of styrene reaching 93.2% and the selectivity for ethylbenzene being 100% only within 20 min. Notably, it also showed good activity even when it was exposed in front air for 1 h before test (Table S3). We ascribed this to the porous nature and highly dispersed Ni particles of this hybrid material, in agreement with the BET, TEM and TOF results. However, the conversions dropped gradually over Ni-Alg-5 and Ni-Alg-10. Only 80.5% conversion was obtained over Ni-Alg-10 under the same reaction conditions, which can be attributed to the destruction of the porous structure and the subsequent Ni particle growths in the reduction process. Moreover, the conversion was 81.1% over Ni/Alg-0, much lower than that of Ni-Alg-0, mainly due to its poor particle dispersion and relatively bigger particle size.

As well known, good catalytic stability is an important feature for an excellent catalyst, and it is also one of the key points for industrial applications. Thus, the stability of Ni-Alg-x and Ni/Alg-0 were investigated in the hydrogenation of styrene for comparison (Fig. 10). As can be seen, both Ni-Alg-5 and Ni-Alg-10 were markedly deactivated after ten runs, although they still showed better stability than Ni/Alg-0, as the conversion of styrene drastically dropped from 81.1% to 65.7% with only five runs over Ni/Alg-0. In contrast, Ni-Alg-0 exhibited excellent stability in the hydrogenation of styrene with the conversion being dropped only 1.9% during ten times of recycling.

Subsequently, the effects of the Ni loadings on the catalytic performances of the hybrid materials were investigated under the same reaction conditions (Fig. 11). It was found that the conversions of styrene were almost 100% over the hybrid materials with over 5.8 wt% Ni loadings, however, the conversion was only around 65.0% over the hybrid material with 3.6 wt% Ni loading. Furthermore, all the hybrid materials with over 3.6 wt% Ni loadings remained stable after ten runs of recycling tests, whereas the conversion of styrene gradually decreased from 67.1% to 62.5% after ten runs over Ni-Alg-0 with 3.6 wt% Ni loading. Notably, when the reaction time was prolonged from 20 to 30 min, the conversion of styrene reached almost 100% over Ni-Alg-0 with 5.8 wt% Ni load-

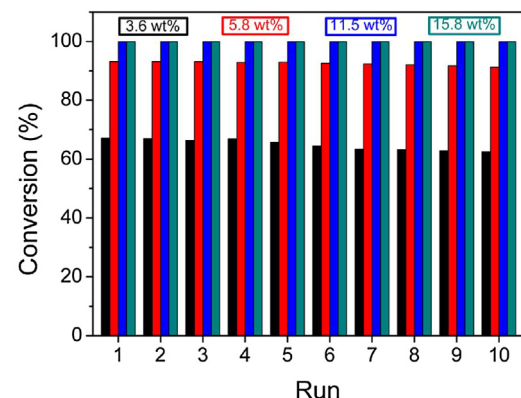


Fig. 11. Reusability results of catalysts with different Ni loadings. Reaction conditions: styrene (42 mmol), catalyst (0.36 g), ethanol (40 mL), $P(H_2)=2$ MPa, 300 rpm, 100 °C, 20 min.

ing, and further experiments indicated it can be reused for 20 times with no significant loss of its initial catalytic activity (Fig. S5), better than most of the previously reported catalytic systems (Table S4). Thus, the Ni-Alg-0 with 5.8 wt% Ni loading was chosen for further study due to the efficiency and cost.

In order to explore the leaching behaviors in catalysts during reactions, ICP analysis on the samples of the comparative experiments (refer to SM for details) were carried out. The results (Figs. S6 and S7) showed that the leaching content of nickel in Ni-Alg-0 was only 1.85 µg/mL (0.35 wt% of total Ni), much lower than that of Ni/Alg-0 (27.14 µg/mL, 5.2 wt% of total Ni). Furthermore, Ni(0) was believed as the main leaching species during the recycling (Fig. S8, Table S2). The leaching behaviors and the changes in structural properties of Ni-Alg-0 and Ni/Alg-0 after recycling (Tables S5 and S6) can further reveal the reasons for the good stability of Ni-Alg-0.

For the excellent catalytic performance of Ni-Alg-0, we think there should be two main reasons: (i) the coordination of Ni(II) ions with Alg in the gelation stage can control the reduction rate of Ni(II) ions, resulting in good dispersion, small particle size, and then good catalytic activity of Ni particles (ii) the strong interaction between Ni particles and Alg in Ni-Alg-0 can suppress agglomeration and prevent loss of the active Ni species during the hydrogenation reaction, resulting in its excellent stability.

In order to evaluate the versatility of Ni-Alg-0, a series of unsaturated substrates was investigated under the same reaction conditions as styrene unless specially noted (Table 2). It was obvious that Ni-Alg-0 exhibited good catalytic activities with over 88.0% conversions for all substrates. Particularly, the conversions of cinnamic acid, cinnamic alcohol, and cyclohexene can reach over 95.0% within one hour with approximately 100% selectivity for the olefinic double bond hydrogenated products. High conversions can also be obtained in nitrobenzene and benzonitrile hydrogenation with aniline (86.1%) and benzylamine (78.0%) being detected as the main products. The results above demonstrated that Ni-Alg-0 possesses good catalytic performance in the hydrogenation of various unsaturated substrates, making it an attractive candidate for practical applications.

4. Conclusions

In conclusion, a novel porous Ni-alginate hybrid material Ni-Alg-0 was firstly prepared via a facile in-situ reduction of Ni(II) alginate 3D hydrogel, which was obtained through the coordination of Ni(II) ions with natural sodium alginate. The coordination between Ni(II) ions and Alg was utilized to modulate the reduction rate of Ni(II) ions, leading to controlled Ni particle sizes and improved dispersion. Notably, Ni(II) species can further be reduced

Table 2

Hydrogenation of various unsaturated substrates over Ni-Alg-0.

Substrates	Main products	Time (min)	Con. (%)	Sel. (%)
		30	>99.9	100
		60	88.5	100
		60	95.7	100
		40	99.7	100
		45	96.3	100
		60	>99.9	86.1
		100	89.6	78.0

Reaction conditions: substrate (42 mmol), ethanol (40 mL), catalyst (0.36 g), P(H₂) = 2 MPa, 300 rpm, 100 °C. ^aCinnamic acid (24.5 mmol), *tert*-butanol (40 mL). ^bNitrobenzene (9.8 mmol).

to Ni(0) to act as the active species in the hybrid material for hydrogenation. Importantly, the morphology and Ni particle sizes of Ni-Alg-x hybrid materials can be tuned by altering solvent component during the reduction process or the Ni loadings. XPS and TGA results demonstrated the strong interaction between Ni and Alg in Ni-Alg-0, which can suppress agglomeration and prevent loss of the Ni species, resulting in its excellent stability in styrene hydrogenation with no appreciable loss of its activity for 20 times of recycling, superior to the conventional supported catalysts in most previous reports. Furthermore, Ni-Alg-0 also exhibited good adaptability in the hydrogenation of various unsaturated substrates. Thus, a new method was established in this work for the fabrication of porous hybrid materials depending on the synergistic effect between nickel and Alg. Owing to the green nature of the starting materials, the simple preparation process and excellent catalytic performance of the obtained hybrid material, it could provide an ideal platform for nanocomposites preparation and design of novel supported catalysts.

Acknowledgments

The authors thank Professor Gang Ma for his kind help.

This work was supported by the National Natural Science Foundation of China (21376060 and 21676068), and the Natural Science Foundation of Hebei Province (B2014201024).

Appendix A. Supplementary data

Supplementary data associated with this article can be found, in the online version, at <http://dx.doi.org/10.1016/j.apcatb.2017.06.088>.

References

- [1] P.H.C. Camargo, Z.Y. Li, Y. Xia, Colloidal building blocks with potential for magnetically configurable photonic crystals, *Soft Matter* 3 (2007) 1215–1222.
- [2] Y. Yan, Y. Dai, S. Wang, X. Jia, H. Yu, Y. Yang, Catalytic applications of alkali-functionalized carbon nanospheres and their supported Pd nanoparticles, *Appl. Catal. B: Environ.* 184 (2016) 104–118.
- [3] K. An, G. Somorjai, Size and shape control of metal nanoparticles for reaction selectivity in catalysis, *ChemCatChem* 4 (2012) 1512–1524.
- [4] J. Du, X. Du, C. Mao, J. Wang, Tailor-made dual pH-sensitive polymer-doxorubicin nanoparticles for efficient anticancer drug delivery, *J. Am. Chem. Soc.* 133 (2011) 17560–17563.
- [5] S.P. Pawar, D.A. Marathe, K. Pattabhi, S. Bose, Electromagnetic interference shielding through MWNT grafted Fe₃O₄ nanoparticles in PC/SAN blends, *J. Mater. Chem. A* 3 (2015) 656–669.
- [6] J. Yu, J. Zhang, M. Jaroniec, Preparation and enhanced visible-light photocatalytic H₂-production activity of CdS quantum dots-sensitized Zn_{1-x}Cd_xS solid solution, *Green Chem.* 12 (2010) 1611–1614.
- [7] N.G. Bastús, F. Merkoçi, J. Piella, V. Puntes, Synthesis of highly monodisperse citrate-stabilized silver nanoparticles of up to 200 nm: kinetic control and catalytic properties, *Chem. Mater.* 26 (2014) 2836–2846.
- [8] Z. Jiang, J. Xie, D. Jiang, J. Jing, H. Qin, Facile route fabrication of nano-Ni core mesoporous-silica shell particles with high catalytic activity towards 4-nitrophenol reduction, *CrystEngComm* 14 (2012) 4601–4611.
- [9] S.H. Joo, J.Y. Park, C.K. Tsung, Y. Yamada, P. Yang, G.A. Somorjai, Thermally stable Pt/mesoporous silica core-shell nanocatalysts for high-temperature reactions, *Nat. Mater.* 8 (2009) 126–131.
- [10] M. Tejamaya, I. Römer, R.C. Merrifield, J.R. Lead, Stability of citrate PVP, and PEG coated silver nanoparticles in ecotoxicology media, *Environ. Sci. Technol.* 46 (2012) 7011–7017.
- [11] W. Feng, H. Dong, L. Niu, X. Wen, L. Huo, G. Bai, A novel Fe₃O₄@nSiO₂@NiPd-PVP@mSiO₂ multi-shell core-shell nanocomposite for cinnamic acid hydrogenation in water, *J. Mater. Chem. A* 3 (2015) 19807–19814.
- [12] G. Bai, X. Wen, Z. Zhao, F. Li, H. Dong, M. Qiu, Chemoselective hydrogenation of benzoic acid over Ni-Zr-B-PEG(800) nanoscale amorphous alloy in water, *Ind. Eng. Chem. Res.* 52 (2013) 2266–2272.

- [13] R. Herbois, S. Noel, B. Leger, L. Bai, A. Roucoux, E. Monflier, A. Ponchel, Cyclodextrins as growth controlling agents for enhancing the catalytic activity of PVP-stabilized Ru(0) nanoparticles, *Chem. Commun.* 48 (2012) 3451–3453.
- [14] H. Li, Y. Xu, H. Yang, F. Zhang, H. Li, Ni-B amorphous alloy deposited on an aminopropyl and methyl co-functionalized SBA-15 as a highly active catalyst for chloronitrobenzene hydrogenation, *J. Mol. Catal. A: Chem.* 307 (2009) 105–114.
- [15] N. Patel, R. Fernandes, S. Gupta, R. Edla, D.C. Kothari, A. Miotello, Co-B catalyst supported over mesoporous silica for hydrogen production by catalytic hydrolysis of ammonia borane: a study on influence of pore structure, *Appl. Catal. B: Environ.* 140–141 (2013) 125–132.
- [16] C. Galeano, R. Güttel, M. Paul, P. Arnal, A.H. Lu, F. Schüth, Yolk-shell gold nanoparticles as model materials for support-effect studies in heterogeneous catalysis: Au@C and Au@ZrO₂ for CO oxidation as an example, *Chem. Eur. J.* 17 (2011) 8434–8439.
- [17] X. Wen, Y. Cao, X. Qiao, L. Niu, L. Huo, G. Bai, Significant effect of base on the improvement of selectivity in the hydrogenation of benzoic acid over Ni/ZrB amorphous alloy supported on γ -Al₂O₃, *Catal. Sci. Technol.* 5 (2015) 3281–3287.
- [18] S. Shang, G. Liu, X. Chai, X. Tao, X. Li, M. Bai, W. Chu, X. Dai, Y. Zhao, Y. Yin, Research on Ni/ γ -Al₂O₃ catalyst for CO₂ reforming of CH₄ prepared by atmospheric pressure glow discharge plasma jet, *Catal. Today* 148 (2009) 268–274.
- [19] W. Li, B. Herkt, M. Seredyck, T.J. Bandosz, Pyridinic-N groups and ultramicropore nanoreactors enhance CO₂ electrochemical reduction on porous carbon catalysts, *Appl. Catal. B: Environ.* 207 (2017) 195–206.
- [20] R. Nie, H. Jiang, X. Lu, D. Zhou, Q. Xia, Highly active electron-deficient Pd clusters on N-doped active carbon for aromatic ring hydrogenation, *Catal. Sci. Technol.* 6 (2016) 1913–1920.
- [21] J.A. Lopez-Sanchez, N. Dimitratos, C. Hammond, G.L. Brett, L. Kesavan, S. White, P. Miedziak, R. Tiruvalam, R.L. Jenkins, A.F. Carley, D. Knight, C.J. Kiely, G.J. Hutchings, Facile removal of stabilizer-ligands from supported gold nanoparticles, *Nat. Chem.* 3 (2011) 551–556.
- [22] J. Ju, W. Chen, In situ growth of surfactant-free gold nanoparticles on nitrogen-doped graphene quantum dots for electrochemical detection of hydrogen peroxide in biological environments, *Anal. Chem.* 87 (2015) 1903–1910.
- [23] Z. Kónya, V.F. Puntes, I. Kiricsi, J. Zhu, J.W. Ager, M.K. Ko, H. Frei, P. Alivisatos, G.A. Somorjai, Synthetic insertion of gold nanoparticles into mesoporous silica, *Chem. Mater.* 15 (2003) 1242–1248.
- [24] Z. Jin, M. Xiao, Z. Bao, P. Wang, J. Wang, A general approach to mesoporous metal oxide microspheres loaded with noble metal nanoparticles, *Angew. Chem. Int. Ed.* 51 (2012) 6406–6410.
- [25] S. Saha, A. Pal, S. Kundu, S. Basu, T. Pal, Photochemical green synthesis of calcium-alginate-stabilized Ag and Au nanoparticles and their catalytic application to 4-nitrophenol reduction, *Langmuir* 26 (2010) 2885–2893.
- [26] S.B. Hammouda, F. Fourcade, A. Assadi, I. Soutrel, N. Adhoum, A. Amrane, L. Monser, Effective heterogeneous electro-fenton process for the degradation of a malodorous compound, indole using iron loaded alginate beads as a reusable catalyst, *Appl. Catal. B: Environ.* 182 (2016) 47–58.
- [27] L. Ai, M. Li, L. Li, Adsorption of methylene blue from aqueous solution with activated carbon/cobalt ferrite/alginate composite beads: kinetics, isotherms, and thermodynamics, *J. Chem. Eng. Data* 56 (2011) 3475–3483.
- [28] L. Ai, J. Jiang, Catalytic reduction of 4-nitrophenol by silver nanoparticles stabilized on environmentally benign macroscopic biopolymer hydrogel, *Bioresour. Technol.* 132 (2013) 374–377.
- [29] F. Shi, L. Mu, P. Yu, J. Hu, L. Zhang, Liquid-phase catalytic hydroxylation of phenol using metal crosslinked alginate catalysts with hydrogen peroxide as an oxidant, *J. Mol. Catal. A: Chem.* 391 (2014) 66–73.
- [30] A. Primo, M. Liebel, F. Quignard, Palladium coordination biopolymer: a versatile access to highly porous dispersed catalyst for suzuki reaction, *Chem. Mater.* 21 (2009) 621–627.
- [31] M. Chitchigovsky, Y. Lin, K. Ouchau, M. Chaumontet, M. Robitzer, F. Quignard, F. Taran, Dramatic effect of the gelling cation on the catalytic performances of alginate-supported palladium nanoparticles for the suzuki-miyaura reaction, *Chem. Mater.* 24 (2012) 1505–1510.
- [32] L. Chen, H. Chen, Y. Li, One-pot synthesis of Pd@MOF composites without the addition of stabilizing agents, *Chem. Commun.* 50 (2014) 14752–14755.
- [33] G. Bai, Z. Zhao, H. Dong, L. Niu, Y. Wang, Q. Chen, A NiPdb-PEG(800) amorphous alloy catalyst for the chemoselective hydrogenation of electron-deficient aromatic substrates, *ChemCatChem* 6 (2014) 655–662.
- [34] Y. Xue, X. Xia, B. Yu, X. Luo, N. Cai, S. Long, F. Yu, A green and facile method for the preparation of a pH-responsive alginate nanogel for subcellular delivery of doxorubicin, *RSC Adv.* 5 (2015) 73416–73423.
- [35] K. Mazur, R. Buchner, M. Bonn, J. Hunger, Hydration of sodium alginate in aqueous solution, *Macromolecules* 47 (2014) 771–776.
- [36] B. Sarker, D.G. Papageorgiou, R. Silva, T. Zehnder, F. Gul-E-Noor, M. Bertmer, J. Kaschta, K. Chrissafis, R. Detsch, A.R. Boccaccini, Fabrication of alginate-gelatin crosslinked hydrogel microcapsules and evaluation of the microstructure and physico-chemical properties, *J. Mater. Chem. B* 2 (2014) 1470–1482.
- [37] B. Li, Y. Dong, C. Zou, Y. Xu, Iron(III)-alginate fiber complex as a highly effective and stable heterogeneous fenton photocatalyst for mineralization of organic dye, *Ind. Eng. Chem. Res.* 53 (2014) 4199–4206.
- [38] Y. Dong, W. Dong, Y. Cao, Z. Han, Z. Ding, Preparation and catalytic activity of Fe alginate gel beads for oxidative degradation of azo dyes under visible light irradiation, *Catal. Today* 175 (2011) 346–355.
- [39] L. Ai, X. Gao, J. Jiang, In situ synthesis of cobalt stabilized on macroscopic biopolymer hydrogel as economical and recyclable catalyst for hydrogen generation from sodium borohydride hydrolysis, *J. Power Sources* 257 (2014) 213–220.
- [40] W. Lin, H. Cheng, J. Ming, Y. Yu, F. Zhao, Deactivation of Ni/TiO₂ catalyst in the hydrogenation of nitrobenzene in water and improvement in its stability by coating a layer of hydrophobic carbon, *J. Catal.* 291 (2012) 149–154.
- [41] Z. Liu, J. Zhou, K. Cao, W. Yang, H. Gao, Y. Wang, H. Li, Highly dispersed nickel loaded on mesoporous silica: one-spot synthesis strategy and high performance as catalysts for methane reforming with carbon dioxide, *Appl. Catal. B: Environ.* 125 (2012) 324–330.
- [42] H. Kim, H.J. Hong, J. Jung, S.H. Kim, J.W. Yang, Degradation of trichloroethylene (TCE) by nanoscale zero-valent iron (nZVI) immobilized in alginate bead, *J. Hazard. Mater.* 176 (2010) 1038–1043.
- [43] H. Li, D. Zhang, G. Li, Y. Xu, Y. Lu, H. Li, Mesoporous Ni-B amorphous alloy microspheres with tunable chamber structure and enhanced hydrogenation activity, *Chem. Commun.* 46 (2010) 791–793.
- [44] J. Zhu, Y. Jia, M. Li, M. Lu, J. Zhu, Carbon nanofibers grown on anatase washecoated cordierite monolith and its supported palladium catalyst for cinnamaldehyde hydrogenation, *Ind. Eng. Chem. Res.* 52 (2013) 1224–1233.
- [45] S. Hu, M. Xue, H. Chen, J. Shen, The effect of surface acidic and basic properties on the hydrogenation of aromatic rings over the supported nickel catalysts, *Chem. Eng. J.* 162 (2010) 371–379.
- [46] L. Ai, H. Yue, J. Jiang, Environmentally friendly light-driven synthesis of Ag nanoparticles in situ grown on magnetically separable biohydrogels as highly active and recyclable catalysts for 4-nitrophenol reduction, *J. Mater. Chem.* 22 (2012) 23447–23453.
- [47] J. Yang, B. Jiang, W. He, Y. Xia, Hydrophobically modified alginate for emulsion of oil in water, *Carbohydr. Polym.* 87 (2012) 1503–1506.
- [48] S.K. Papageorgiou, E.P. Kouvelos, E.P. Favvas, A.A. Sapalidis, G.E. Romanos, F.K. Katsaros, Metal-carboxylate interactions in metal-alginate complexes studied with FTIR spectroscopy, *Carbohydr. Res.* 345 (2010) 469–473.
- [49] H. Ren, Y. Song, Q. Hao, Z. Liu, W. Wang, J. Chen, J. Jiang, Z. Liu, Z. Hao, J. Lu, Highly active and stable Ni-SiO₂ prepared by a complex-decomposition method for pressurized carbon dioxide reforming of methane, *Ind. Eng. Chem. Res.* 53 (2014) 19077–19086.
- [50] J. Ashok, S. Kawi, Nickel-Iron alloy supported over iron–alumina catalysts for steam reforming of biomass tar model compound, *ACS Catal.* 4 (2014) 289–301.
- [51] X. Kang, H. Liu, M. Hou, X. Sun, H. Han, T. Jiang, Z. Zhang, B. Han, Synthesis of supported ultrafine non-noble subnanometer-scale metal particles derived from metal-organic frameworks as highly efficient heterogeneous catalysts, *Angew. Chem. Int. Ed.* 128 (2016) 1092–1096.
- [52] L. Qiu, F. Liu, L. Zhao, W. Yang, J. Yao, Evidence of a unique electron donor-acceptor property for platinum nanoparticles as studied by XPS, *Langmuir* 22 (2006) 4480–4482.
- [53] H. Li, H. Li, W. Dai, W. Wang, Z. Fang, J. Deng, XPS studies on surface electronic characteristics of Ni-B and Ni-P amorphous alloy and its correlation to their catalytic properties, *Appl. Surf. Sci.* 152 (1999) 25–34.
- [54] E. Raymundo-Piñero, F. Leroux, F. Béguin, A high-performance carbon for supercapacitors obtained by carbonization of a seaweed biopolymer, *Adv. Mater.* 18 (2006) 1877–1882.
- [55] P. Parhi, A. Ramanan, A.R. Ray, Preparation and characterization of alginate and hydroxyapatite-based biocomposite, *J. Appl. Polym. Sci.* 102 (2006) 5162–5165.
- [56] M. Ionita, M.A. Pandele, H. Iovu, Sodium alginate/graphene oxide composite films with enhanced thermal and mechanical properties, *Carbohydr. Polym.* 94 (2013) 339–344.
- [57] J. Liu, C. Li, F. Wang, S. He, H. Chen, Y. Zhao, M. Wei, D.G. Evans, X. Duan, Enhanced low-temperature activity of CO₂ methanation over highly-dispersed Ni/TiO₂ catalyst, *Catal. Sci. Technol.* 3 (2013) 2627–2633.
- [58] W. Lin, H. Cheng, L. He, Y. Yu, F. Zhao, High performance of Ir-promoted Ni/TiO₂ catalyst toward the selective hydrogenation of cinnamaldehyde, *J. Catal.* 303 (2013) 110–116.
- [59] M. Zhu, G. Diao, Synthesis of porous Fe₃O₄ nanospheres and its application for the catalytic degradation of xylenol orange, *J. Phys. Chem. C* 115 (2011) 18923–18934.